Fluid simulations of tokamak turbulence in quasiballooning coordinates

A. M. Dimits
Lawrence Livermore National Laboratory, Livermore, California 94550
(Received 24 May 1993)

A set of coordinates for simulations in toroidal magnetic geometry, called quasiballooning coordinates, is proposed and implemented. Quasiballooning coordinates are straight-field-line coordinates in which one of the coordinate directions is as close as possible to that of the magnetic field consistent with the near-parallel grid lines meshing exactly (without interpolation) as they cross the boundaries of the simulation region. This allows the true periodicity conditions in the toroidal-poloidal plane to be satisfied in a straightforward and seamless way, even for sheared magnetic fields. Quasiballooning coordinates are useful in the simulation of instabilities and turbulence of interest in fusion plasmas since the number of grid cells needed to represent structures that are elongated along the magnetic field with a given resolution is greatly reduced compared with toroidal-poloidal or other nontwisting coordinates. For explicit codes, they allow shorter time steps, and it is anticipated that for particle codes, their use will naturally minimize the numerical noise. The key details necessary for the implementation of quasiballooning coordinates, both in finite-difference and pseudospectral fluid codes are presented, and a fluid code has been written. The advantages of quasiballooning coordinates are demonstrated by applying this code to turbulence driven by the $v'_{\parallel}$ instability.

PACS number(s): 02.70.−c, 52.65.+z, 52.35.−g, 52.55.Fa

I. INTRODUCTION

Many instabilities of interest in tokamak plasmas, such as ion-temperature-gradient-driven (ITG) modes, trapped-electron modes, and pressure-driven magnetohydrodynamic modes, have a mode structure which is highly elongated along the equilibrium magnetic field. ITG modes, for example, have $k_{\parallel}/k_{\perp} \sim \rho_i/L_T$ [1], where $k_{\parallel}$ and $k_{\perp}$ are the wave numbers, respectively, along and perpendicular to the magnetic field, ρ_i is the thermally averaged ion gyroradius, and L_T is the gradient scale length of the background temperature profile. The elongation direction (i.e., the direction of the magnetic field) is generally neither purely toroidal nor poloidal. Coordinates that are aligned with the magnetic-field lines have been used widely in linear analysis [2–4], and in some calculations of equilibria [5]. There are now numerous three-dimensional nonlinear simulation studies of instabilities and turbulence in the published literature. Recent examples include fluid simulations [6,7] and particle simulations [8,9] of ITG-driven turbulence, fluid simulations of trapped-electron-driven turbulence [10], and fluid simulations of resistive kink modes [11]. Most of these simulations have either used coordinates aligned with the poloidal and toroidal directions [7,8,11], or have ignored or significantly altered the periodicity conditions that the fluctuation fields actually satisfy [6,9]. An exception is the work of Carreras *et al.*, in which purely spectral representations in the toroidal-poloidal surfaces of the fields were used. The convolution calculations needed to calculate the nonlinear terms in this last approach are expensive and impose much more severe limits on the resolution attainable than would a configuration-space based approach in which the nonlinearities are local.

To understand that standard toroidal-poloidal grids are tremendously wasteful of grid resolution, consider Figs. 1. The grid cell size needed to resolve a structure is given by the requirement that some number (of order 1) grid cells fit entirely inside the structure. Thus, for typical values of the magnetic safety factor $q \sim 1$, a much finer grid is needed in "standard" toroidal-poloidal coordinates [Fig. 1(a)] than in "ballooning coordinates" [Fig. 1(b)], in which one of the coordinates is exactly aligned with the magnetic field. The ratio of the number of grid cells needed to resolve an elongated structure in standard vs ballooning coordinates is approximately a_s/a_b, where a_s is the aspect ratio of the structure and a_b is the aspect ratio of the toroidal-poloidal domain. For the ITG instability in fusion devices, for example, this ratio is typically of order 100. Ballooning coordinates have the disadvantage, however, that the toroidal-poloidal periodicity conditions are difficult to implement satisfactorily. In Fig. 1(b), the top of the elliptical structure that crosses the boundary lies on a grid line on the right-hand-side of the boundary, but not on the left. In order to use ballooning coordinates, some form of interpolation is needed to make the connection across the boundary. While this approach merits investigation, it has the disadvantage that the numerical representation of the fields and operators in the region near the boundary where the interpolation is done is different from that in the rest of toroidal-poloidal plane.

Here, nonlinear simulation methods that use what will be termed "quasiballooning coordinates," are introduced and developed. In quasiballooning coordinates, one of the coordinate directions lies approximately (*not necessarily exactly*) along the magnetic field. A lack of alignment is allowed which has a negligible effect on the reso-

lution, but permits the implementation of the correct periodicity conditions via exact offset-periodic meshing of the grid lines at opposite ends of the simulation region [Fig. 1(c)]. Quasiballooning coordinates allow calculations in configuration space. Since most plasma nonlinear terms are local or nearly local in configuration space, their computation is much cheaper there than in wave-number space. Finite-difference and discrete-Fourier methods are both applicable within each radial surface. For fluid or Vlasov-fluid-type simulations, the reduction in computer time needed per time step decreases in proportion to or more rapidly than the decrease in the number of grid cells needed. Also, in many cases, the coarse parallel grid automatically filters out physically irrelevant but numerically problematic high-frequency modes, permitting much longer time steps for explicit time stepping, in both particle and fluid codes.

In this paper, grid representations and applications to fluid simulations in slab geometry are discussed in detail. In addition to the work reported here, a toroidal partially linearized gyrokinetic particle code that uses quasiballooning coordinates has been developed. This will be reported on in future publications.

The outline of the paper is as follows. In Sec. II the basic coordinate system is defined and its resolution properties discussed. Methods for calculating radial derivatives when the coordinate system is allowed to twist to follow a sheared magnetic field are discussed in Sec. III.

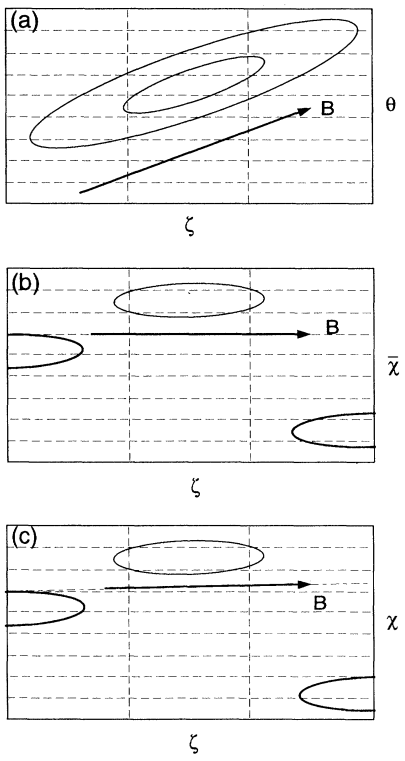

FIG. 1. Grid (dotted lines), magnetic field (arrows), and turbulent structures (ellipses) at a single radial location, as seen in (a) toroidal-poloidal coordinates, (b) ballooning coordinates, and (c) quasiballooning coordinates.

In Sec. IV, the application of discrete Fourier representations and fast Fourier transforms in quasiballooning coordinates is considered. Section V describes some details that were not covered in previous sections of a fluid code in which quasiballooning coordinates were implemented. The implementation of radial boundary conditions, in particular, is discussed there. In Sec. VI, the primary advantages of quasiballooning coordinates are demonstrated by comparing the results of simulations of parallel-velocity-gradient ($V'_{\|0}$) driven turbulence in which quasiballooning coordinates are used to results in which toroidal-poloidal and other (more optimized) nontwisted coordinates are used. Finally, the results of this paper are summarized and discussed in Sec. VII.

II. BASIC METHOD

Let V, θ, and ζ be radial, poloidal, and toroidal straight-field-line coordinates, such as Hamada coordinates [12], normalized so that their values range from 0 to 1. A suitable coordinate choice is (V,χ,ζ), where $\chi \equiv \theta - \hat{\iota}(V)\zeta$. Here, $\hat{\iota}(V) \simeq \iota(V)$ where $\iota(V)$ is the magnetic rotational transform. The periodicity conditions that a field ψ must satisfy are

$$\psi(V,\chi+1,\zeta)=\psi(V,\chi,\zeta) , \tag{1a}$$

$$\psi(V,\chi-\hat{\iota},\zeta+1)=\psi(V,\chi,\zeta) . \tag{1b}$$

The second of these is the one that causes the complication in ballooning coordinates, in which $\hat{\iota}(V)$ is chosen to be identically equal to $\iota(V)$. Quasiballooning coordinates can be obtained as follows: The V and χ coordinates are discretized on a mesh $V_i=(i-1)/N_V$, $\chi_j=(j-1)/N_\chi$, where $i=1,2,\ldots,N_V$, and $j=1,2,\ldots,N_\chi$. While the discretization of χ needs to be uniform, there is no such requirement on the discretization of V. At each radial mesh surface, $V=V_i$ an integer $m(i)$ is chosen that to minimize $\iota(V_i)-\hat{\iota}(i)$, where $\hat{\iota}(i)\equiv m(i)/N_\chi$. The periodicity condition at the $\zeta=0,1$ boundary is exactly satisfied by setting

$$\psi(i,j-m(i),1)=\psi(i,j,0) . \tag{1c}$$

Both the continuous and discrete periodicity conditions, given respectively by Eqs. (1b) and (1c), are one to one since they map each radial (V) surface to itself with a shift [$\hat{\iota}(V)$ or $m(i)$] which is constant on each radial surface.

The parallel derivative at $V=V_i$ is given by

$$\nabla_{\|i}=\frac{\partial}{\partial\zeta}+[\iota(V_i)-\hat{\iota}(i)]\partial/\partial\chi .$$

It is straightforward to show that the resolution loss due to the difference between $\hat{\iota}$ and ι is negligible. For a highly elongated structure, we have $\partial/\partial\theta \gg \nabla_\|$. Our choice of $\hat{\iota}$ satisfies $|\hat{\iota}-\iota| \le 1/(2N_\chi)$, while the shortest length scale that is resolved by the χ mesh is $1/N_\chi$. The maximum discretized (eigen)value of $(\iota-\hat{\iota})(\partial/\partial\chi)$ is therefore comparable to 1, so that the number of mesh surfaces N_ζ needed in the ζ direction is set only by the parallel length scales of the structure. This is the optimal situation, i.e., ballooning coordinates, in which $\hat{\iota}=\iota$ iden-

tically, are no better. In toroidal-poloidal coordinates ($\hat{\iota}=0$, $\chi=\theta$, and $\nabla_\parallel=\partial/\partial\zeta+\iota\partial/\partial\theta$), the resolution of the poloidal (θ) mesh is wasted unless $N_\zeta \gtrsim N_\theta=N_\chi$, since typically $\iota=O(1)$, in tokamak plasmas. The reduction in the number of grid points that can be attained is proportional to the elongation of the structures along the magnetic field in the normalized toroidal-poloidal plane. For ITG turbulence, for example, a reduction of order 10^{-2} is to be expected.

There is a possible intermediate choice of coordinates that can be used. These will be called "nontwisted-quasiballooning" coordinates. Here, $\hat{\iota}$ is chosen to be independent of V and to match $\iota(V)$ at a single V (preferably at or near the middle of the simulation region). It will be shown that for sheared magnetic fields, the restriction that $\hat{\iota}$ be independent of V causes a significant degradation in the resolution relative to quasiballooning coordinates, even if the radial extent of the simulation region is much smaller than the profile gradient scale lengths.

In the large-aspect-ratio torus limit, the choice of coordinates described above is nearly orthogonal. This takes care of the calculation of the discretization of the component of the perpendicular derivative in a magnetic surface, since

$$\frac{\hat{\mathbf{b}}\times\nabla V}{|\nabla V|}\cdot\nabla=[1+O(\epsilon^2)]\frac{\partial}{\partial\chi} ,$$

where $\hat{\mathbf{b}}$ is the unit vector in the direction of the magnetic field and ϵ is the inverse aspect ratio.

It is possible to use the same idea and transform ζ instead of θ. One then deals with $\hat{q}(i)=m(i)/N_\zeta$ instead of $\hat{\iota}$. The quasiparallel coordinate is then θ. This choice may have some advantages, since the periodicity conditions in the toroidal direction, which is the symmetry direction, are unaltered by the transformation. The disadvantage of this choice is that the resulting coordinates are highly nonorthogonal, even in the large-aspect-ratio limit, although an expansion in the aspect ratio of the turbulent structures may render the effects of this nonorthogonality small in some cases.

The above formulation is directly applicable to simulations of a full cross section of a tokamak or to a thin toroidal annulus (i.e., region that is of small extent in V). There have been several simulation studies that have used various forms of "flux-tube" geometry [16]. In these cases, the simulation region is a long thin tube (usually of rectangular cross section) centered on a single magnetic-field line. The long axis of the tube is along the field line. The particular implementations have used either nontwisted coordinates or ballooning coordinates. The boundary conditions are usually taken to be periodic in the direction along the magnetic field and in the direction perpendicular to the field and the equilibrium gradients. The validity of results from simulations using such geometries must be tested by changing the size of the simulation region in order to verify that there are spatial correlation lengths that are shorter than the system size in each direction. If this can be done, then such geometries offer much better poloidal resolution than thin-annulus or full-cross-section geometries. The disadvantages are that the tests must be done *a posteriori,* and that they cannot easily be used to investigate situations where the fluctuations have multiple components of which one or more have a long correlation length in some direction.

Quasiballooning coordinates and the other constructions discussed in the subsequent sections of this paper are equally useful for simulations in a flux-tube geometry. To apply them to this geometry, the domain L_χ of χ is viewed as being much smaller than the poloidal extent of the torus. If we take $L_\chi=2\pi/M_\chi$, where M_χ is an integer, then ι is replaced by the effective rotational transform $\iota_{\rm ft}\equiv\iota M_\chi$ for the smaller domain in doing the above coordinate and periodicity constructions. Any poloidal-angle dependence of equilibrium quantities that is present in the physical model equations used is then taken to be a function of the parallel coordinate only. Quasiballooning coordinates, with the associated offset periodic connection in the quasiparallel direction, then yield the correct physical periodicity conditions in the parallel direction. The independence of the simulation results on the size of the simulation region then only needs to be checked explicitly for the directions perpendicular to the magnetic field, but not for the parallel direction. Furthermore, the radial derivative construction given in the next section guarantees that poloidal grid resolution does not degrade as a function of ζ because of the decrease in the radial separation of the constant-χ mesh surfaces as a function of ζ.

The implementation of quasiballooning coordinates is quite straightforward and the main issues involved for fluid (finite-difference and pseudospectral) codes are addressed in the next three sections. The main restriction on the $\iota(V)$ profiles that can be used is that they be reasonably smooth.

III. RADIAL DERIVATIVES

Radial derivatives are involved in nonlinear terms, finite-gyroradius terms, and diffusion terms. In order to use any twisted coordinate system, including quasiballooning coordinates, it is necessary to have valid discretizations of any radial derivatives that are needed. These discretizations should be consistent with the correct physical periodicity conditions and should have some (grid-scale) symmetry in the toroidal angle. Consider, for example, the radial first derivative

$$\left.\frac{\partial\psi}{\partial V}\right|_\theta=\left.\frac{\partial\psi}{\partial V}\right|_\chi-\zeta\hat{\iota}'(V)\frac{\partial\psi}{\partial\chi} . \tag{2}$$

Since $\partial\psi/\partial V|_\theta$ is continuous across the $\zeta=0$, $\zeta=1$ boundary, it follows that $\partial\psi/\partial V|_\chi$ is generally discontinuous. If the two terms on the right-hand side of Eq. (2) are discretized separately, then there is generally no guarantee that the discontinuities would cancel. Furthermore, as one moves along a field line, $\partial/\partial V|_\chi$ increasingly points in the poloidal direction, so that resolution in the χ direction is lost. As an example, consider the common situation where the ion Larmor radius ρ_i sets a minimum spatial scale of physical interest. If the poloidal resolution is set at ρ_i at one value of the parallel

coordinate, then the grid points involved in the discretization of $\partial\psi/\partial V|_\chi$ may become a distance greater than ρ_i apart. The radial derivative expression then becomes inaccurate for structures of size ρ_i in the χ direction. This resolution loss can be very large either for structures that are much more elongated in the radial direction than in the poloidal direction or in flux tube geometries where the variation in $\iota_{\rm ft}$ with radius is large because of the small perpendicular extent of the system. Also, the dependence on parallel coordinate introduces a fake linear coupling. Furthermore, as will be discussed in Sec. V, discontinuities in the discretization across the parallel boundary can lead to fast phenomena that cause numerical problems.

A better procedure, which avoids these problems, is to discretize the radial derivative directly. The radial difference of a field Ψ on a (V,χ) mesh line (i,j) is formed from quantities $\hat{\psi}$ that represent values of the field at different radial locations $i\pm1$, $i\pm2$, etc., but at the same value of θ (not χ). Since this value of θ generally lies in between the χ mesh surfaces, the $\hat{\psi}$'s must be constructed by interpolation in χ. Figure 2 shows the intersections of constant-V and -χ surfaces with the $\zeta=0$ surface (a) and with a $\zeta\neq0$ surface (b), viewed in (V,θ) configuration space. The lines for which θ is equal to the value at the grid node at which the difference is being taken are shown. Their intersections with the adjacent radial surfaces do not coincide with those of the constant-χ mesh surfaces. Stated formally, a discretization is used that has the form

$$[\Delta\Psi]_{i,j,k}=\sum_l \alpha_l \hat{\psi}(i+l,\theta[i,j,k],k)\ , \tag{3}$$

where $\theta[i,j,k]$ denotes the value of θ at the (V,θ,ζ) index values (i,j,k). Since $\theta[i,j,k]$ in general lies between grid lines at radial surface $i+l$ unless $l=0$, interpolation between values of ψ at the grid points is used to determine $\hat{\psi}$. For the resulting difference formula to not have discontinuities in the ζ (or in the k index), an interpolation scheme, such as splines, of at least one order higher than the derivative needed should be used. Alternatively, a Fourier representation in χ provides a natural interpolation scheme with infinite-finite-order accuracy.

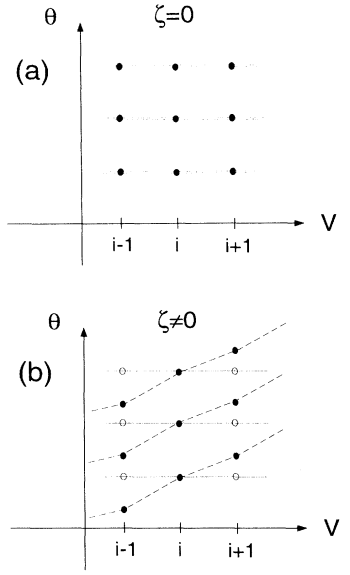

FIG. 2. Intersections of constant-V and -χ surfaces with the $\zeta=0$ surface (a) and with a $\zeta\neq0$ surface (b), viewed in configuration (V,θ) space. Lines for which θ is equal to the value at the grid node at which the difference is being taken are shown. The solid dots are the intersections of the grid lines with the constant-ζ surfaces, the open circles are the points at which the fields are needed for the radial differences, the solid lines are lines of constant θ and the dotted lines are lines of constant ζ.

As a simple illustration, the result obtained by this procedure for a centered-difference approximation to a radial first derivative, using linear interpolation in χ, is

$$\hat{\Delta}_V|_\theta\psi(i,j,\zeta)=\frac{1}{2\Delta V}\{\psi(i+1,j,\zeta)-\psi(i-1,j,\zeta)+\zeta(\psi[i+1,j+m(i+1)-m(i),\zeta]-\psi[i+1,j,\zeta])$$
$$+\zeta(\psi[i-1,j,\zeta]-\psi[i-1,j+m(i-1)-m(i),\zeta])\}\ . \tag{4}$$

The first line of terms on the right-hand side can be identified as the centered-difference discretization of $\partial\psi/\partial V|_\chi$, while the remaining terms are a discretization of $\zeta\hat{\iota}'(V)\partial\psi/\partial\chi$. Equation (4), as an approximation to Eq. (2), is second-order accurate in N_V^{-1} and first-order accurate in N_χ^{-1}. It is defined for all values of ζ between 0 and 1, and is therefore defined when ζ is discretized on a mesh. In practice, one would use either a spline of at least quadratic order or a Fourier representation to do the interpolation in χ so that the interpolation errors are not inherently larger than the errors inherent in the difference formula.

The $\mathbf{E}\times\mathbf{B}$ advection nonlinearity has the property that its form is unaltered by the transformation to quasiballooning coordinates. The respective nonlinear terms have the form

$$\nabla_\perp\cdot(\boldsymbol{V}_{EB}f)=[\phi,f]+O(\epsilon^2)\ ,$$

where $\boldsymbol{V}_{EB}\equiv\hat{\mathbf{b}}\times\nabla_\perp\phi$ is some $\mathbf{E}\times\mathbf{B}$-like velocity, ϕ is some potential function, and ϵ is the local inverse aspect ratio and

$$[\phi,f]\equiv\frac{\partial}{\partial V}\left[\phi\frac{\partial f}{\partial\theta}\right]-\frac{\partial}{\partial\theta}\left[\phi\frac{\partial f}{\partial V}\right]\ . \tag{5a}$$

For any value of S, the transformation $(V,\theta,\zeta)\rightarrow(V,Y,\zeta)$, where

$$Y\equiv\theta-\hat{\iota}(V)S$$

preserves the form of $[\phi,f]$. That is,

$$[\phi,f]=[\phi,f]_s$$
$$\equiv\frac{\partial}{\partial V}\left[\phi\frac{\partial f}{\partial Y}\right]-\frac{\partial}{\partial Y}\left[\phi\frac{\partial f}{\partial V}\right]. \tag{5b}$$

The V derivatives are with θ fixed in Eq. (5a) and with Y fixed in Eq. (5b). This offers at least three alternative possibilities for the discretization of such nonlinear terms: (i) The first possibility is to set $S=\zeta$, so that $Y=\chi$ and discretize the last form directly. Although this is formally uniformly accurate to the order of the differencing formula used, it suffers from loss of resolution away from $\zeta=0$ and results in an expression that is discontinuous across the $\zeta=0-1$ boundary. We have tried this method in the fluid code discussed below and found that unless the perpendicular diffusion is large enough to ensure very high grid accuracy, a discontinuity is produced in the fields at the $z=0-1$ boundary that results in very large parallel diffusion rates. This in turn produces severe timestep constraints in an explicit code. (ii) The second possibility results from noting that Eqs. (5) hold for any value of S. At each z, choose $S_1(i)$ and $S_2(i)$ such that $S_1(i)\le\zeta\le S_2(i)$, and such that $N_\chi[\hat{\iota}(i)-\hat{\iota}(i-1)]S_1(i)$, $N_\chi[\hat{\iota}(i)-\hat{\iota}(i-1)]S_2(i)$, $N_\chi[\hat{\iota}(i+1)-\hat{\iota}(i)]S_1(i)$, and $N_\chi[\hat{\iota}(i+1)-\hat{\iota}(i)]S_2(i)$ are all integers. Because of the choice of S_1 and S_2, no interpolation is needed to calculate $[\phi,f]_{S_1}$ and $[\phi,f]_{S_2}$. The nonlinear term at $S=\zeta$ is then calculated using interpolation in ζ between S_1 and S_2 using $[\phi,f]_{S_1}$ and $[\phi,f]_{S_2}$. This method seems to offer interesting possibilities. An important question is whether the requirement on the values of S is too restrictive to allow sufficiently accurate interpolation. (iii) The third possible method is to use Eq. (5a) directly, together with the derivative construction of the form of Eq. (3). This is the option that has been most used in the fluid code discussed below.

IV. FOURIER METHODS

Methods based on Fourier expansions have several potential advantages over finite-difference methods and other local discretization schemes. For smooth fields, Fourier expansions converge more rapidly as the number of basis functions increases. They also diagonalize many common differential and integral operators. These properties motivate an investigation of the applicability of Fourier methods in quasiballooning coordinates.

First, Fourier transforms (and therefore discrete Fourier transforms) in χ are taken in the same way as for θ since the periodicity conditions on χ are the same as those on θ.

In order to use Fourier representations to calculate parallel derivatives and wave numbers, the Fourier transform with respect to ζ is required. Since the coordinate transformation alters the periodicity conditions with respect to ζ, the Fourier transform with respect to ζ is also altered. Fast Fourier transforms can still be used to do this transform. Consider the field $\psi(k_\chi,l)$ where l is the discrete index for $\zeta_l\equiv(l-1)/N_\zeta$, where N_ζ is the number of mesh points in the ζ direction. (The radial variable has been suppressed). The discrete Fourier transform of $\psi(k_\chi,l)$ is defined by

$$\psi(k_\chi,k_\zeta)\equiv\sum_{l=1}^{MN_\zeta}\psi(k_\chi,l)\exp(-2\pi ik_\zeta l/MN_\zeta),$$

where M is the number of passages made by a $\chi=$const grid line in the ζ direction before it loops back on itself. Using the periodicity condition $\psi(k_\chi,l+N_\zeta)=\exp(2\pi ik_\chi\hat{\iota})\psi(k_\chi,l)$, it follows that

$$\psi(k_\chi,k_\zeta)=M\sum_{\xi=1}^{N_\zeta}\exp(-2\pi im\xi/N_\chi)\times[\exp(-2\pi ik_\chi\hat{\iota}\xi/N_\chi)\psi(k_\chi,\xi)],$$

where the allowed values of k_ζ are given by $k_\zeta=M(m+k_\chi\hat{\iota})$. Note that $M\hat{\iota}$ is an integer that represents the number of passages made by a $\chi=$const grid line in the χ direction before it loops back on itself. Discrete Fourier transforms in the radial direction can also be used in a similar way. Once the field is available in k_χ space, it can be multiplied by a phase factor that represents a transformation from χ to θ, so that a radial Fourier transform becomes a sum of fields evaluated at the same θ. Differential and integral operators that are simple in (k_V,k_χ) can then be applied before transforming back from k_V to V and multiplying by a phase factor to transform from θ to χ.

V. SIMULATION CODE AND BOUNDARY CONDITIONS

In order to demonstrate the properties and advantages of quasiballooning coordinates, a three-dimensional explicit finite-difference fluid code has been written that can be switched to use either toroidal-poloidal, nontwisted-quasiballooning, or full quasiballooning coordinates. The simulation region is periodic in the θ and ζ directions. The boundary and periodicity conditions, viewed in physical space, are independent of the choice of coordinates. Their representation in the two sets of coordinates is, of course, different. Two different sets of radial boundary conditions were implemented.

In the first, the quasiballooning radial coordinate is made periodic. In physical space, this corresponds to connecting the radial boundaries in such a way that at $z=0$, the radial boundary conditions are periodic, while at other values of z, there is a displacement in y that makes the magnetic field orientation appear continuous across the radial boundary. (The small difference between quasiballooning and ballooning coordinates can be viewed as resulting in a small change in the ι profile near the boundary. If desired this change can be eliminated by imposing a slight restriction on L_s.) This boundary condition reduces to a radially periodic boundary condition in the absence of magnetic shear.

This boundary condition is equivalent to one that has been implemented by Kotschenreuther and Wong [13] and can be called the "twist-shift periodic radial" (TSPR) boundary condition. It can be used in either of two ways. One can use parameters such that $\hat{\iota}(1)-\hat{\iota}(0)$ is an integer. Provided that this is compatible with the equilibrium, as in a simulation of slab physics or in a flux tube geometry,

in ballooning or quasiballooning coordinates, this completely eliminates any radial discontinuity. This choice does not generally make sense for a toroidal annulus geometry for typical parameter values, since the change in the rotational transform over a short radial distance is usually much less than 1. The second alternative is to let $\hat{\iota}(1)-\hat{\iota}(0)$ be arbitrary. In this case, there are discontinuities, for example, in particle orbits if they cross both the radial and quasiparallel boundaries. Even though the details of the nonlinear spectrum are then affected by the presence of the radial boundary, the TSPR boundary condition may still leave the turbulence sufficiently intact to allow enough transport to prevent substantial quasilinear relaxation. There is a possibility of numerical instabilities associated with the discontinuity. If these are not prohibitive, then this boundary condition may still be useful.

The TSPR boundary condition has also been implemented in toroidal-poloidal and nontwisted-quasiballooning coordinate versions of the code. In this case, an explicit poloidal offset is used. There is then a jump in the orientation of the box sides across the radial boundary, as shown in Fig. 3. The jump in the box orientation corresponds to a jump in the toroidal-poloidal wavenumber spectrum across the boundary, although individual modes that are common to both sides of the boundary are continuous across the boundary. The implementation is much simpler in true (twisting) quasiballooning coordinates.

Finally, it is important to note that in a toroidal annulus geometry, this periodicity condition is incompatible with the equilibrium poloidal dependence of any toroidal terms.

The second choice of boundary conditions is to set the fields to zero at the radial boundary and to prevent quasilinear relaxation by damping the fields with a damping coefficient that is finite and strong enough to suppress the turbulence close to the boundaries, but goes smoothly to zero at some finite distance from the boundaries. In the simulation code discussed in the next section, the specific form used is

$$\gamma(V)=\gamma_0\times\begin{cases}(V-a)^2/a^2, & 0<V<a\\ 0, & a\le V\le 1-a\\ [V-(1-a)]^2/a^2, & 1-a<V<1\ .\end{cases} \tag{6}$$

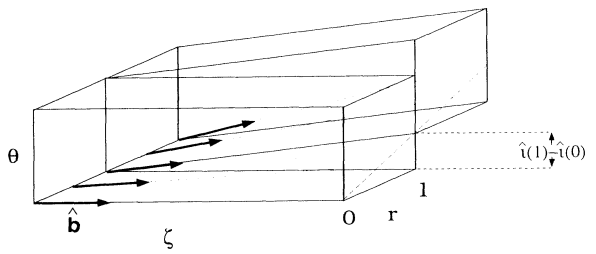

FIG. 3. TSPR boundary conditions. At the radial boundary $r=1$, the replica simulation boxes are connected with an offset in θ such that the magnetic field is continuous across the boundary, and so that the magnetic field is (quasi-) parallel with the ζ axis just to the right of the radial boundary in each periodic replica. The heavy arrows denote the magnetic-field direction.

This coefficient has a finite value γ_0 at the radial boundaries $V=0$ and 1, and goes smoothly to zero at a finite distance $a\lesssim 0.3$ from the walls. In this case, the momentum flux is controlled by the damping rate and width of the damping layer.

The resultant damping terms result in effective sources near the boundaries that prevent quasilinear relaxation. If the turbulence has a finite intrinsic radial correlation length, independent of the distance between the radial boundaries, then it is possible to maximize the momentum flux at a level that is independent of the damping layer width, by making the damping rate and layer width much larger than the radial correlation length of the turbulence. In practice, however, this is difficult since the radial extent of the simulation region necessary to do this is significantly greater than that of the undamped region (by at least a factor of 3—more if the damping rate and layer width is not correctly optimized) because of the presence of the two damping layers. It is sufficient if the quasilinear relaxation in the undamped region is incomplete, provided that the mean gradients in the partially relaxed fields can be measured with reasonable accuracy.

VI. FLUID EXAMPLE: LONG-WAVELENGTH $V'_{\parallel 0}$-DRIVEN TURBULENCE

A. Equations

In this section, results of simulations of long-wavelength turbulence driven by the "drift-Kelvin-Helmholtz" (DKH) or parallel-ion-velocity-driven ($V'_{\parallel 0}$) instability [14,15] are presented that demonstrate the advantages of quasiballooning coordinates. In this section, the notation has been changed from that of the previous sections according to $(V,\theta,\zeta)\rightarrow(x,y,z)$. The following model fluid equations are used:

$$\frac{\partial\phi}{\partial t}+\frac{1}{\eta_v}\frac{\partial\phi}{\partial y}=-\alpha\nabla_\parallel v_\parallel+D_x\frac{\partial^2\phi}{\partial x^2}+D_y\frac{\partial^2\phi}{\partial y^2}+\alpha^2 D_\parallel\nabla_\parallel^2\phi\ , \tag{7a}$$

$$\frac{\partial v_\parallel}{\partial t}+V_{EB}\cdot\nabla_\perp v_\parallel=-\frac{\partial\phi}{\partial y}-\alpha\nabla_\parallel(2\phi)+\mu_x\frac{\partial^2 v_\parallel}{\partial x^2}+\mu_y\frac{\partial^2 v_\parallel}{\partial y^2}+\alpha^2\mu_\parallel\nabla_\parallel^2 v_\parallel\ , \tag{7b}$$

where

$$V_{EB}\equiv-\nabla_\perp\phi\times\hat{\mathbf{z}}\ ,$$

$$\nabla_\parallel\equiv\frac{\partial}{\partial z}+\left[\iota_c+\frac{x-0.5}{\alpha L_s}\right]\frac{\partial}{\partial y}\ ,$$

$$\alpha\equiv\frac{L_v}{\rho_i}\frac{r}{R}\ ,$$

ϕ is the electrostatic potential, $v_\parallel$ is the perturbed parallel velocity, D_x, D_y, $D_\parallel$, μ_x, μ_y, and $\mu_\parallel$ are diffusion coefficients, and r and R are the minor and major radii. The normalizations are $\phi\sim(T_0/e)(L_x/L_v)$, $T\sim T_0(L_x/L_v)$, $v_\parallel\sim v_{ti}(L_x/L_v)$, $x\sim L_x$, $y\sim L_y$, $z\sim L_z$,

$L_s \sim L_v L_x/\rho_i$, and $t \sim L_v L_y/(v_{ti}\rho_i)$, where T_0 is the equilibrium temperature of the ions and electrons (assumed to be equal), e is the ion charge (taken to be the negative of the electron charge), the equilibrium parallel velocity profile is taken to be $V_{\|0}(x)=v_{ti}x/L_v$, L_x is an arbitrary radial length scale that satisfies $\rho_i \ll L_x \ll L_v$, $L_y=2\pi r$, and $L_z=2\pi R$, where $v_{ti}=\sqrt{T_0/m}$ is the ion thermal velocity, m is the ion mass, and $\eta_v=L_n/L_v$, where $L_n=-[d\ln n_0(x)/dx]^{-1}$, and $n_0(x)$ is the equilibrium density. Equation (7a) is obtained from the ion density evolution equation, combined with quasineutrality and adiabatic electron response. Equation (7b) is obtained from the ion parallel momentum equation. Linearly, these equations are subject to the DKH instability if $\eta_v > \sqrt{2}$. Saturation of the instability can occur due to nonlinear $\mathbf{E}\times\mathbf{B}$ advection of the parallel velocity, which is described by the second term in Eq. (7b). The normalized radial flux of parallel velocity and the effective diffusivity are given by $\Gamma_v(x,t)=\chi_v=\langle V_{EBx}v_\| \rangle$, where V_{EBx} is the x component of $\mathbf{V}_{EB}$, with the normalizations $\Gamma_v \sim \rho_i v_{ti}(v_{ti}/L_v)(L_x/L_y)(L_x/L_v)$ and $\chi_v \sim \rho_i v_{ti}(L_x/L_y)(L_x/L_v)$. The angle brackets denote an average over y and z. These equations also require for their validity that $\rho_i \nabla_\perp \ll 1$ for the perturbed quantities.

Equations (7) and their basic scalings are similar to those of a model for ITG turbulence that has been considered in some detail [7]. They are solved using the code described in the previous subsection.

B. Results

The radially local behavior ($L_s=\infty$) is considered here first. The parameter values used were $\boldsymbol{\mu}=\mathbf{D}$, $D_x=0.015$, $D_y=0.002$, $D_\|=0.001$, $\eta_v=\infty$, and $\alpha=5$. The number of grid cells in the x and y directions was $(N_x,N_y)=(59,127)$. The number of grid cells in the z direction was varied on a case-by-case basis. Here, the "z direction" refers to the toroidal direction in toroidal-poloidal coordinates and to the quasiparallel direction in quasiballooning coordinates. The simulations in this set are radially bounded with damping near the boundaries given by $\gamma_0=300$ and $a=0.3$. Figure 4 shows results from a simulation run with $N_z=29$ that used quasiballooning coordinates. For this case, since ι is independent of position, the coordinate system does not twist (i.e., $\hat{\iota}$ is independent of x).

The instability has grown through a linear phase to a nonlinearity saturated state with partial (not complete) quasilinear relaxation of the $v_\|$ profile [Fig. 4(b)] and a nonzero parallel velocity flux [Fig. 4(a)] that is carried through the system by the turbulence. The potential contours show structures that are extended in the radial direction [Fig. 4(c)] and in the parallel direction [Fig. 4(d)]. When a simulation with the same parameter values is attempted in toroidal-poloidal coordinates, no instability or turbulence is observed. Because of inadequate toroidal resolution, there are no linearly unstable modes.

The advantage of quasiballooning coordinates can perhaps be seen most clearly in the scaling of the number of grid cells needed with α. For the present demonstration runs, the moderate value $\alpha=5$ has been chosen.

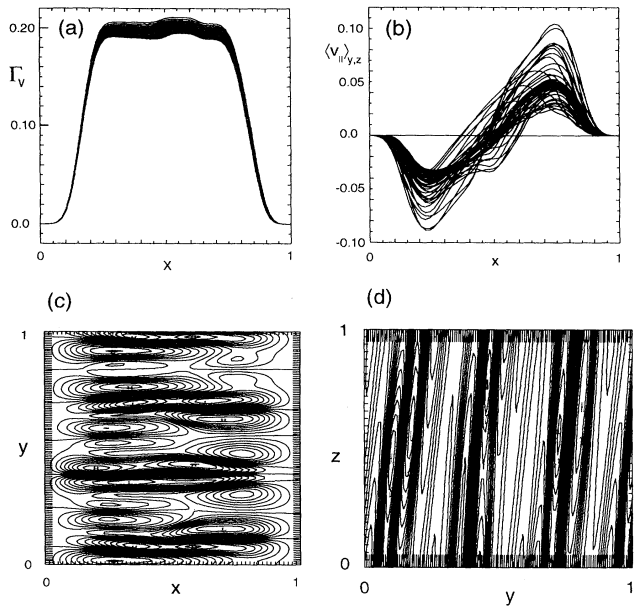

FIG. 4. (a) Profile of the radial flux of parallel velocity averaged over y and z, and over time intervals of $\Delta t=0.2$ at times $16 \le t \le 24$; (b) profile of $v_\|$ averaged as in (a); (c) potential contours in a x-y cut; and (d) potential contours in a y-z cut at $t=24$ from a bounded simulation with $L_s=\infty$ and $\iota_c=0.5586$, with $x=0.49$, done in quasiballooning coordinates.

Even for this value, far fewer grid cells are needed in quasiballooning coordinates than in toroidal-poloidal coordinates. When quasiballooning coordinates are used, the normalized momentum flux converges as a function of N_z to a value of 0.12, and this value is attained for $N_z=15$. In contrast, when toroidal-poloidal coordinates are used, convergence is not achieved even for $N_z=59$. In actual experiments, α is typically of order 100. The number of structures per box length in the y direction increases strongly as a function of α [7]. If α is increased, keeping ι and $\hat{\iota}$ fixed with $\iota-\hat{\iota} \gtrsim 1/\alpha$, then the number of grid cells needed in the toroidal direction is directly proportional to the number needed in the y direction. The number of structures per period in the parallel direction, and therefore the number of grid cells needed in the quasiparallel direction in quasiballooning coordinates, however, scales as $1/\alpha$ times the number of structures in the y direction. The ratio of the number of grid cells needed in toroidal-poloidal coordinates to the number needed in quasiballooning coordinates therefore increases roughly in proportion to α.

In order to attempt to empirically verify the dependence of the number of grid cells necessary on α and ι, a series of simulation runs was done in which α and ι were varied from the values given above. An effort was made to increase N_z until two values of N_z gave the same behavior and flux levels, indicating convergence. This was done for $\iota_c=0.26$, 0.55, and 0.97, with $\alpha=5$ and for $\iota_c=0.55$ with $\alpha=10$. The diffusion coefficients and edge damping rate were chosen so that the respective terms in Eqs. (7) increased in proportion to α. The results are

TABLE I. Dependence of the normalized diffusivity for $v_\parallel$ on α, ι, and N_z, from a series of unsheared-slab simulation runs of $v'_\parallel$ turbulence. Values of $\chi=0$ indicate that the particular simulation was linearly stable. The figures given with a "±" indicate that the flux changed as a function of time about a mean value, with a spread given by the second number. In the other cases, the momentum flux was steady to within $\lesssim 3\%$.

		χ			
α	ι	$N_z=7$	χ, $N_z=15$	$N_z=29$	$N_z=59$
		toroidal-poloidal coordinates			
5	0.26	0.20	0.14±0.02	0.38	0.30
5	0.55	0	0	0.60	
5	0.97	0	0.80	0.30	
10	0.55	0	0	0.15	
		quasiballooning coordinates			
5	0.26	0.27	0.29	0.29	
5	0.55	0.20±0.02	0.19	0.20	0.20
5	0.97	0.72	0.65	0.60	
10	0.55	0.09±0.03	0.12±0.05	0.12±0.05	

summarized in Table I. They partially confirm the above reasoning, and show that quasiballooning coordinates are superior. With quasiballooning coordinates, reasonable convergence is achieved with $N_z=15$ for all of the parameter choices. With toroidal-poloidal coordinates, some indication of convergence was only seen for the $\alpha=5$, $\iota=0.26$ case. For all of the cases with ι above 0.26 convergence was not achieved for $n_z \lesssim 59$.

In explicit codes, it is anticipated that shorter time steps can be used since physically stable and unwanted high-frequency modes that are present when toroidal-poloidal or nontwisted coordinates are used are automatically removed. This was verified for the linear phase of the simulation runs. For $N_z=29$ and 59 and for several α and ι sets, simulation runs were made for increasing values of the time step (starting from a given value and doubling) until numerical instability was observed in the linear phase of the simulation. The maximum stable timestep is given in Table II. It did not depend on N_z for the values used. This time step was larger for the quasiballooning coordinate cases and decreases for the largest values of α and ι used. The range of values scanned does not, however, permit a clear scaling behavior to be discerned.

It was not possible to see a clear dependence in the time step on coordinate systems for the nonlinear phase. This is because for the moderate parameter values used in the simulation runs of the previous section, the shortest time scales that set the maximum time step appear to be associated with the nonlinear terms. Even for these moderate parameter values, very large simulation runs are needed to achieve converged results for the toroidal-poloidal coordinate cases. The time-scale separation between the unwanted high-frequency stable modes and the physically relevant turbulence will increases with α. To see the increase in the usable time steps in a comparison between simulations using quasiballooning coordinates and other coordinates, simulations with larger (more realistic) values of α and hence more poloidal grid cells are needed. The computer resources needed to run the toroidal-poloidal coordinate cases, are therefore prohibitive due to the grid-cell number requirements. It is important to note that in physical models that include electron dynamics, the highest frequencies will be considerably higher. The natural optimization of the frequency spectrum by quasiballooning coordinates may then be crucial.

TABLE II. Maximum stable time step for the linear phase of simulations with the values of α and ι given. TP denotes the toroidal-poloidal coordinate simulations, and QB denotes the quasiballooning coordinate simulations.

		τ	
ι	α	TP	QB
0.56	5	0.001	0.002
0.56	10	0.001	0.002
0.97	5	0.001	0.002
0.97	10	0.0005	0.002

The differences between full quasiballooning coordinates and nontwisted quasiballooning coordinates for a situation with magnetic shear will now be discussed. If $\hat{\iota}$ is independent of x, then the condition $\iota-\hat{\iota}\lesssim 1/\alpha$ can only hold over a radial distance for which $\Delta\iota \simeq \Delta x\, d\iota/dx \lesssim 1/\alpha$. The scale Δx defined in this way is just the two-dimensional slab shear- (or Landau-) damping distance. Even if one is interested in simulating a region whose radial thickness is much less than the profile gradient scale lengths, a key issue in determining the transport is whether or not the radial correlation lengths are determined by two-dimensional slab processes or by toroidal or three-dimensional processes. In the linear theory of toroidal modes, such as the toroidal ITG mode, linear toroidal coupling can produce unstable modes that have radial extents much greater than the two-dimensional slab shear damping scale (but still smaller than the profile gradient scales). To address such questions the radial extent of the simulation region must be many (or at least several) times larger than the two-dimensional slab shear damping scale. The number of grid cells needed in a code that uses full twisting quasibal-

looning coordinates is therefore reduced in comparison to a code in which the coordinate system does not twist by a factor of order the radial extent of the system divided by the two-dimensional slab shear- (or Landau) localization distance.

To demonstrate this point, we examine the behavior of simulations with strong magnetic shear with quasiperiodic radial boundary conditions. The parameters used are similar to those used above, with the following exceptions. The ι profile used is $\iota(x)=\iota_c+(x-0.5)/(\alpha L_s)$, with $\iota_c=0.5586$ (chosen arbitrarily) and $L_s=0.1$. The values of the diffusion coefficients are $D_x=0.01$, $D_y=0.001$, and $D_z=0.0005$. The number of grid cells in the z direction is again varied to determine the resolution requirements. When run in quasiballooning coordinates, the steady-state momentum flux was converged at $\Gamma_v=0.012$, with $N_z=15$. Essentially no change in the flux level, the field contours, nor in the overall evolution was seen if N_z was increased to $N_z=29$ or 57. Figure 5 shows radial profiles of the momentum flux and of the quasilinear component of the perturbed parallel velocity, as well as contours of $|\phi|$ in the $x-y$ plane, with $N_z=29$. In contrast, when the simulations are repeated using nontwisted quasiballooning coordinates, the results are not converged with respect to N_z even for $N_z=119$. The radial profiles of Γ_v at times much later than those of Fig. 5 for various values of N_x are shown in Fig. 6.

VII. CONCLUSIONS

A set of coordinates for simulations in toroidal magnetic geometry, called quasiballooning coordinates, has been proposed and implemented. Quasiballooning coordinates are straight-field-line coordinates in which one of the coordinate directions as close as possible to that of the magnetic field consistent with the quasiparallel grid lines meshing exactly, without interpolation, as they cross the boundaries of the simulation region.

Quasiballooning coordinates are useful in the simulation of many instabilities (and the resulting turbulence) of interest in fusion plasmas since for structures that are elongated along the magnetic field, the number of grid cells needed for a given resolution is reduced by a factor of order the elongation of the structures compared with the number needed in toroidal-poloidal coordinates. Thus, they retain the full resolution advantages of ballooning coordinates, in which one of the coordinate directions is exactly aligned with that of the magnetic field, but allow the true periodicity conditions in the toroidal-poloidal plane to be satisfied in a straightforward and seamless way, even in the presence of magnetic shear. For many instabilities of fusion interest, the elongation along the magnetic field is very large and so, therefore, is the advantage of using quasiballooning coordinates. If the magnetic field is sheared, then the quasiballooning coordinates must twist with the magnetic field. Even if the coordinates are aligned with the magnetic field at one position but do not twist, then the number of grid cells needed for a given resolution is increased by a factor proportional to the number of two-dimensional shear-damping localization widths contained in the system. This number can be large even if the radial extent of the system is much less than the equilibrium gradient scale lengths and must be large in order for a simulation to address the radial correlation lengths, and therefore the transport levels, in a toroidal plasma.

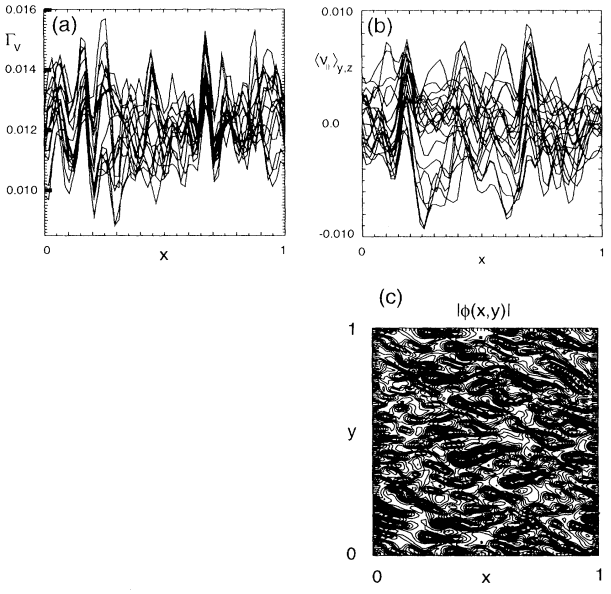

FIG. 5. (a) Profiles of Γ_v, (b) profiles of the quasilinear component of the $v_{\|}$ (c) contours of ϕ in the x-y plane, and from a fluid simulation using quasiballooning coordinates with $\iota=0.5586$, at $x=0.5$, $L_s=0.1$, and $N_z=29$. The profiles are averaged as in Fig. 4, with the time intervals $\Delta t=0.1$ and are for $6\le t\le 8$.

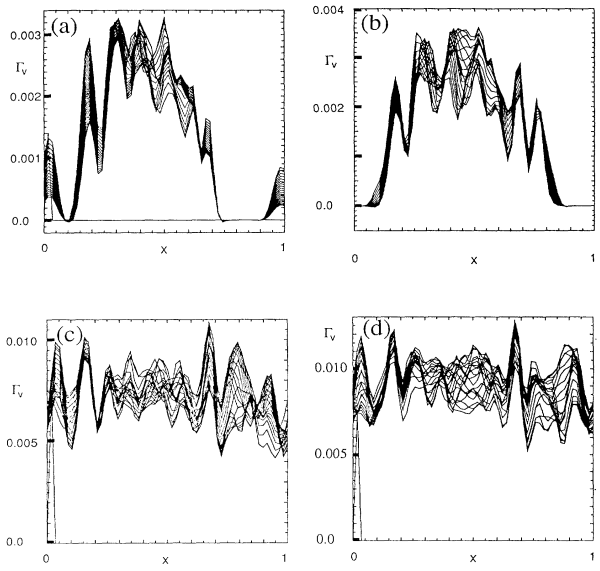

FIG. 6. Profiles of Γ_v at late times $(10\le t<12)$ for (a) $N_z=15$, (b) $N_z=29$, (c) $N_z=59$, and (d) $N_z=119$, from simulation runs done in nontwisted coordinates. The parameters are as for Fig. 5, except for the values of N_z, which are shown.

Along with the direct reduction in the number of grid cells needed, there are other advantages to using quasiballooning coordinates. In explicit codes, it is expected that shorter timesteps can be used since physically stable and unwanted high-frequency modes that are present when toroidal-poloidal or nontwisted coordinates are used are automatically removed. This was verified for the linear phase of the simulation runs, although comparisons for the nonlinear phase are prohibitive due to the computer resources needed for any of the nonquasiballooning-coordinate cases. Also, in particle codes, the unwanted high-frequency modes contribute to the noise spectrum, so that their removal is expected to result in a significant reduction in the numerical noise. This point will be examined in a future presentation.

The key details necessary for the implementation of quasiballooning coordinates, both in finite-difference and pseudospectral fluid codes have been addressed. A fluid code was written that uses quasiballooning coordinates, and the above points were demonstrated by applying the code in fluid simulations of the $v'_{\parallel}$ instability and turbulence.

This work represents a beginning in the use of quasiballooning coordinates. We have also implemented quasiballooning coordinates in a partially linearized gyrokinetic particle code. The details and results will be presented elsewhere. There are many instabilities and turbulent processes in toroidal plasmas whose study will be made much easier with a quasiballooning coordinates.

There are two important issues to be addressed to determine the general applicability of quasiballooning coordinates. The first is their usefulness for electromagnetic perturbations. If such fluctuations are of small amplitude, so that there is a "nearby" equilibrium with good flux surfaces, then the methods given in this paper can be applied directly. If, however, there are large-amplitude magnetic perturbations, then the coordinate system will have to be allowed to evolve in time. The second is the case where the transformation between standard spatial coordinates and straight-field-line coordinates is singular, for example if there is a separatrix in the poloidal field. This case requires special treatment. These are topics of current research and will be reported in future presentations.

ACKNOWLEDGMENTS

The author gratefully acknowledges useful discussions with T. M. Antonsen, Jr., S. C. Cowley, J. F. Drake, P. N. Guzdar, R. H. Cohen, L. LoDestro, G. Hammett, S. Parker, and M. Kotschenreuther. A fluid code written by J. F. Drake and P. N. Guzdar [7] was the starting point for the code developed for this paper. This work was performed by LLNL for the U.S. DOE under Contract No. W-7405-ENG-48.

[1] B. Coppi, M. N. Rosenbluth, and R. Z. Sagdeev, Phys. Fluids **10**, 582 (1967).

[2] J. W. Connor, R. J. Hastie, and J. B. Taylor, Phys. Rev. Lett. **40**, 396 (1978).

[3] A. H. Glasser, in *Proceedings of the Finite-β Theory Workshop, Vienna, 1977,* edited by B. Coppi and W. Sadowski (U.S. Department of Energy Report No. CONF-7709167, Washington, D.C., 1977), p. 55.

[4] Y. C. Lee and J. W. Van Dam, in *Proceedings of the Finite-β Theory Workshop, Vienna, 1977* (Ref. [3]), p. 93.

[5] A. Reiman and H. Greenside, Comput. Phys. Commun. **43**, 157 (1986).

[6] S. Hamaguchi and W. Horton, Phys. Fluids B **2**, 1833 (1990).

[7] J. F. Drake, P. N. Guzdar, and A. M. Dimits, Phys. Fluids B **3**, 1937 (1991).

[8] M. J. Lebrun, T. Tajima, M. G. Gray, G. Furnish, and W. Horton, Phys. Fluids B **5**, 752 (1993).

[9] B. I. Cohen, T. J. Williams, A. M. Dimits, and J. A. Byers, Phys. Fluids B **5**, 2967 (1993).

[10] B. A. Carreras, K. Sidikman, P. H. Diamond, P. W. Terry, and L. Garcia, Phys. Fluids B **4**, 3115 (1992).

[11] R. G. Kleva and J. F. Drake, Phys. Fluids B **3**, 372 (1991).

[12] S. Hamada, Nucl. Fusion **2**, 23 (1962).

[13] M. Kotschenreuther and H. V. Wong (private communication).

[14] N. D'Angelo, Phys. Fluids **8**, 1748 (1965).

[15] P. J. Catto, M. N. Rosenbluth, and C. S. Liu, Phys. Fluids **16**, 1719 (1973).

[16] S. C. Cowley (private communication); P. N. Guzdar (private communication); G. Hammett (private communication); S. Parker (private communication).